International Global Navigation Satellite Systems Association
IGNSS Conference 2016

Colombo Theatres, Kensington Campus, UNSW Australia
6 – 8 December 2016

Local augmentation to wide area PPP systems: a case study in Victoria, Australia

Ken Harima
School of Science, RMIT University, Australia
Phone: +61 3 9925 3775 Email: ken.harima@rmit.edu.au
Suelynn Choy
School of Science, RMIT University, Australia
Phone: +61 3 9925 2650 Email: suelynn.choy@rmit.edu.au
Luis Elneser
Position Partners Pty. Ltd., Australia
Phone: +61 3 9708 9900 Email: LElneser@positionpartners.com.au
Satoshi Kogure
Space Technology Directorate, Japan Aerospace Exploration Agency, Japan
Phone: +81 50 3362 3558 Email: kogure.satoshi@jaxa.jp

ABSTRACT

Precise GNSS positioning services and infrastructure are becoming increasingly important to support precise positioning applications for machine control in mining, civil construction, agriculture, and transport. Currently these applications are serviced by Real-time Kinematic (RTK) services relying on dense GNSS tracking networks. These services are impractical to deploy over wide areas or for applications in remote areas such as hydrographic surveying. Precise Point Positioning (PPP) have demonstrated potential to deliver centimetre-level accuracy without the onerous requirement of ground GNSS network. However PPP requires solution convergence times in the order of tens of minutes compared to the few seconds with RTK. A wide area (national or regional level) GNSS positioning infrastructure should consist of a sparse wide area reference network for PPP and complemented by dense local networks supporting RTK-like systems where practical. The wide area infrastructure is used for computation of precise satellite orbits, clocks and signal biases while the local network is used to derive atmospheric corrections required for rapid convergence. This paper presents the results this type of PPP-RTK system which uses existing global correction streams, i.e., JAXA's MADOCA and CNES's CLK91, and local ionospheric corrections derived from these streams using Victoria's GPSnet network stations. Observables from individual stations and the global corrections were used to estimate tropospheric and ionospheric delays. The computed ionospheric delays were then used to generate local ionospheric correction maps for each GPS satellite. Real-time tests using GPS and GLONASS satellites were performed at 5 GPSnet CORS stations. Results show that PPP-RTK type system using local ionospheric corrections can significantly reduce the solution convergence times and positioning errors in PPP

KEYWORDS: Precise Point Positioning (PPP); Rapid convergence; ionospheric corrections;

1. INTRODUCTION

Demands for reliable, high accuracy positioning services have been steady rising over recent years. Activities like the use of machine guidance and control in mining, agriculture, civil construction and transport require high accuracy position. As the demands for these services become more wide spread, positioning infrastructure necessary to support these services must be considered.

Most of the currently established high accuracy positioning services are based on differential positioning techniques like Real-Time Kinematic (RTK). These services account for systematic biases by comparing the observations from the user receiver with those obtained from a nearby reference station. While RTK can provide centimetre-level accuracy with convergence times shorter than a few minutes, the requirement of reference station in close proximity to the user makes the prospect of establishing nation-wide or region-wide infrastructures for RTK services impractical.

The Precise Point Positioning (PPP) technique, is considered a promising alternative to differential positioning techniques. PPP has already demonstrated its capability of producing decimetre-level accuracies (Kouba, 2009; Zumberge et al., 1997) and centimetre-level accuracies when ambiguity resolution is performed (Ge et al., 2007, Laurichesse et. al 2009). The requirement for PPP services is the timely transmission of precise satellite orbits and clock corrections as well as the GNSS measurement biases. Because these parameters for PPP are global valid, they can be measured using a sparse, global network of continuously operating reference station (CORS). This makes PPP an ideal algorithm to provide high accuracy services over large areas.

A combination of PPP based position and satellite based delivery will be independent of local infrastructure, making it ideal for supporting positioning and navigation applications where local infrastructure is either unavailable or unreliable. This includes oceans, remote areas but also can be conceived in the aftermath of natural disasters.

However, one disadvantage of PPP is that it requires some time for the solutions to converge to centimetre level accuracy. It typically requires in the order of tens of minutes. When rapid to instantaneous convergence is required, differential techniques like RTK are still the best mode for positioning.

A practical solution for providing wide area high accuracy positioning service is to combine RTK-like services whereby local GNSS infrastructure is available with PPP services as a backdrop providing wide area solutions. In order for receivers to seamlessly transition from one solution to the other, the global corrections for PPP and local corrections for RTK-like systems should be made compatible.

Recent studies have demonstrated that local atmospheric corrections, calculated using measurements from a dense network of reference stations can significantly reduce the solution convergence times (Zhang et al., 2013, Li et. al 2015). By calculating ionospheric corrections and tropospheric corrections alongside the satellite orbits, satellite clocks and signal biases from the network side, and transmitting these corrections to the end user, a convergence time of a few minutes can be obtained.

The studies mentioned above as well as the availability of global real-time messages suited for PPP (IGS 2015), allows the possibility to implement and test locally enhanced PPP systems based on GNSS augmentation messages containing State Space Representation corrections. In this type of system, global messages for PPP will be calculated from the global reference networks, while local messages containing mainly atmospheric corrections, will be generated using local reference station networks.

In the work presented herein, ionosphere assisted PPP (PPP+Ion) solutions, computed from local ionospheric delay corrections, along with publicly available global PPP correction products are calculated and evaluated. The global real-time satellite products, i.e., the CLK91 stream, generated by the French Space Agency (CNES, 2016); and the MADOCA stream, generated by the Japanese Aerospace Exploration Agency (JAXA, 2016) are used as the global products.

2. PPP AND IONOSPHERIC CORRECTIONS

In contrast with differential techniques like RTK, which accounts for errors in the GNSS signals by taking the difference between observation on the receiver and reference station, PPP relies on robust modelling of the errors. The errors in the carrier phase and pseudorange GNSS measurements are modelled as,

$$P_1 = \rho + Mt_r^s T_r + I_r^s + (dt_r - dt^s) + (B_1^s - B_{1r}) \quad (1.1)$$

$$P_2 = \rho + Mt_r^s T_r + \mu_2 I_r^s + (dt_r - dt^s) + (B_2^s - B_{2r}) \quad (1.2)$$

$$L_1 = \rho + Mt_r^s T_r - I_{1_r}^{\ s} + (dt_r - dt^s) + \lambda_1 N_1 + (b_1^s - b_{1r}) + d\varphi_r^s \quad (2.1)$$

$$L_2 = \rho + Mt_r^s T_r - \mu_2 I_r^s + (dt_r - dt^s) + \lambda_2 N_2 + (b_2^s - b_{2r}) + d\varphi_r^s \quad (2.2)$$

where, P_i and Li are the pseudorange and carrier phase measurements on L1 and L2 frequencies; dt^s is the satellite clock correction B_i^s is the satellite code biases, and b_i^s is the satellite phase biases calculated using the global reference station networks. $d\varphi_r^s$ includes the modelled carrier phase errors such as phase windup effect and antenna PCVs. Global mapping functions (GMF) in (Boehm et. al 2006) were used to estimate the troposphere delay factor Mt_r^s. The Geometric range ρ, tropospheric zenith delay T_r, receiver clock dt_r and the carrier phase ambiguities N_i are parameters to be estimated. The receiver code and phase bias B_{ir} and b_{ir} are absorbed by the ambiguity estimates and eliminated using satellite single difference prior to ambiguity resolution.

2.1 PPP algorithm

The earliest algorithms for PPP (Zumberge et al., 1997) rely on the iono-free combination to eliminate the effect of ionospheric error I_r^s.

$$P_{IF} + dt^s + B_{IF}^s = \rho + dt'_r + Mt_r^s T_r \quad (3)$$

$$L_{IF} + dt^s + b_{IF}^s - d\varphi_r^s = \rho + dt'_r + Mt_r^s T_r + \lambda_{NL} N_{NL} - c_2 \lambda_2 N_{WL} \quad (4)$$

In (3) and (4), P_{IF} and L_{IF} are the iono-free linear combination of pseudoranges and carrier phase measurement, respectively. The ionospheric error has already been eliminated by forming the iono-free combination. The iono-free combination of receiver code biases will be absorbed by the receiver clock estimate, while the receiver phase a biases and geometry free component of receiver code biases will be absorbed by the "narrow-lane" and "wide-lane" ambiguities N_{NL} and N_{WL}. N_{NL} contains the ambiguity N_1 and a linear combination of receiver biases, N_{WL} contains the difference between N_1 and N_2 biases as well as a linear combination

of receiver biases.

The first attempt to perform ambiguity resolution used the Melbourne-Wubenna combination to isolate the ambiguities N_{NL} and N_{WL} (Ge et al., 2007),

$$P_{MW} + B^s_{MW} - pw^s_{MW} = \lambda_{WL}(N_1 - N_2) + B_{MWr} \quad (5)$$

In (5), P_{MW} is the Melbourne-Wubenna combination of pseudorange and carrier phase measurements. B_{MWr} is the Melbourne-Wubenna combination of code and phase biases and pw^s_{MW} is a correction term to account for the effect of phase windup in the Melbourne-Wubenna measurement. Because B_{MWr} is common to all satellites, the satellite-differenced Melbourne-Wubenna combination can be used to solve the single differenced (N_1-N_2) ambiguity. Solving the correct ambiguity of the (N_1-N_2) using (5) can be reliably achieved in a few minutes (Laurichesse et. al 2009) even when using the simple integer-rounding technique.

Because receiver biases affect all satellite equally, the single differenced N_{WL} ambiguity can be replaced by the solved (N_1-N_2) ambiguity once this is done. The single differenced N_{NL} can be estimated alongside the geometric distance, receiver clock and tropospheric zenith delay. The resolution of the N_{NL}, or single differenced N_1 ambiguity was performed using the modified LAMBDA algorithms in (Chang et. al, 2009). It is the estimation of this ambiguity that takes tens of minutes to a few hours, which results in the long convergence time in PPP.

The present work uses this technique to obtain PPP results at user-end. For the locally enhanced PPP+Ion solutions, a fourth combination, the geometry-free combination of carrier phases, is used to both measure and use slant ionospheric delays. Use of locally measured slant delays will aid the estimation of the N_1 ambiguity and thus shorten convergence times for PPP.

2.2 Ionospheric delay measurement and assimilation

Using ionosphere-free combinations like (3), (4) and (5) isolates the estimation of ambiguities from the effects of ionospheric delays. This would normally preclude the estimation or utilization of ionospheric corrections in the PPP algorithm. The relationship between the ionospheric delays, and ambiguities can be easily established using the geometry free combination of carrier phase measurements,

$$L_{GF} + b^s_{GF} - pw^s_{GF} = I^s_r/c_2 + (\lambda_1 - \lambda_2)N_{NL} + \lambda_2 N_{WL} \quad (6)$$

For reference stations networks, the ionospheric correction can be calculated using (6) and estimates of ambiguities N_{NL} and N_{WL}. With both N_{NL} and N_{WL} resolved, the measurement errors for the single differenced ionospheric delay will be the single differenced geometry-free combination of carrier phase noise. It is assumed that the rover receiver will use the same phase bias corrections b^s_{GF} and phase windup model to calculate pw^s_{GF}, the effect of phase windup on the geometry free combination.

On the rover receiver, (6) can be used in conjunction with an external ionospheric delay estimate to aid the ambiguity estimation and accelerate convergence. In particular, after the N_{WL} ambiguity has been resolved, (6) directly relates the geometry free measurement with the ambiguity N_{NL}. Assuming a carrier phase noise of 1cm, the measurement error for (6) will be 2cm and 0.65 times the ionosphere error. The wavelength accompanying the N_{NL} is 5.4cm, which makes it difficult to resolve the ambiguity almost instantaneously. The end user should

be able to estimate the ambiguity N_{NL} to within one cycle as long as the accuracy of the single difference ionosphere correction is better than 5 cm. This combined with (4) should lead to decimetre-level position accuracy, with a shorter convergence time

3. CASE STUDY IN VICTORIA AUSTRALIA

PPP solutions were calculated using 16 stations belonging to the GPSnet CORS network. The PPP results and geometry free measurement were used to estimate slant ionospheric delays at each of the 16 stations. The ionospheric delays were then used to calculate ionosphere assisted PPP (PPP+Ion) solutions for 5 station belonging to the same CORS network.

3.1 Slant Ionosphere estimation

Both reference station side and receiver side used the global products CLK91 from CNES and MADOCA products from JAXA, to obtain PPP solutions and attempt resolution of N_{NL} and N_{WL} ambiguities. Table 1 shows the content of the CLK91 and MADOCA corrections for GPS and GLONASS satellites.

	Sat. Clock	Sat. orbit	Code/Phase. Bias	URA
CLK91 GPS	**5 sec.**	**5 sec.**	**5 sec.**	**-**
CLK91 GLO	**5 sec.**	**5 sec.**	**5 sec.**	**-**
MADOCA GPS	**1 sec.**	**30 sec.**	**30 sec.**	**30 sec.**
MADOCA GLO	**1 sec.**	**30 sec.**	**30 sec.**	**30 sec.**

Table 1 Content of CLK91 and MADOCA corrections

Although the MADOCA products also contain PPP corrections for the Japanese QZSS satellite, the selected stations did not support real-time streaming of measurements from QZSS satellite. For this reason, corrections for QZSS satellite were not used in this research. It is also to note that although both products contain phase biases to allow ambiguity resolution, the MADOCA products are yet to reach maturity, and thus the ambiguity resolution rate for N_{NL} was low when using the MADOCA products.

The stations used in the tests presented here are shown in Figure 1 and the stations information is presented in Table 2. ionospheric delays were calculated in all 16 stations for both global products. Station positions were modelled as constant unknown variables corrected for solid Earth tides and FES2004 ocean tide loading; station clocks as random variables with no constraints; tropospheric zenith delays were modelled as random walk variables with a variability of 0.1mm/second; the ambiguities were modelled as constant unknown variables. Integer rounding was used to resolve N_{WL} ambiguities; a modified LAMBDA (Chang, 2005) method was used for N_{NL} ambiguity resolution.

Position solutions using PPP and PPP+Ion methods were calculated for the fixed stations EBNK, LCLA, MAFF, WORI and YALL, here forth called monitoring stations. These stations are represented by red dots in Figure 1. The PPP settings for these solutions were the same as those for the other stations except the following: receiver position was modelled as a random variable, and ocean tide loading was not applied.

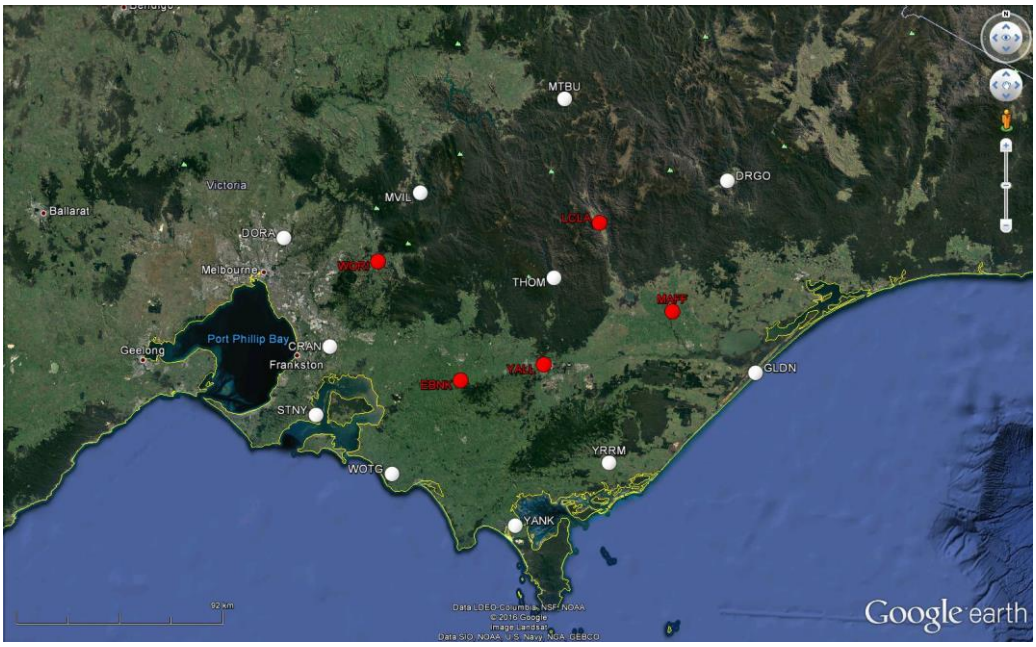

Figure 1 Monitoring Network. Ionospheric delays were calculated for both red and white stations. The PPP and PPP+Ion solutions were calculated for the red stations.

For the PPP+Ion solution, an ionospheric delay estimate was interpolated from values calculated at stations within 150km (the ionospheric delay estimates from the monitoring station itself were not used) as will be explained in the next section.

Name	Latitude (ITRF08)	Longitude (ITRF08)	Height	Antenna	Receiver
CRAN	-38.107984611	145.286925389	63.814	TRM59800.00	Trim. netR9
DORA	-37.680851111	145.064431000	141.108	TRM29659.00	Trim. netR9
DRGO	-37.459129194	147.251487056	221.286	LEIAX1202GG	Leic. GRX1200GG
EBNK	-38.243506389	145.936040833	181.842	TRM57971.00	Trim. netR9
GLDN	-38.208863583	147.402748056	25.163	TRM57971.00	Trim. netR5
LCLA	-37.628203278	146.622299250	210.020	TRM57971.00	Trim. netR5
MAFF	-37.972179972	146.985297139	42.634	TRM57971.00	Trim. netR5
MTBU	-37.145128972	146.448786417	1600.569	TRM29659.00	Trim. netR9
MVIL	-37.510234528	145.740768611	457.913	TRM57971.00	Trim. netR5
STNY	-38.375176111	145.214038667	29.205	LEIAR25.R3	Leic. GRX1200+
THOM	-37.843532306	146.398237139	479.696	TRM57971.00	Trim. netR5
WORI	-37.777066500	145.530033139	117.854	TRM57971.00	Trim. netR9
WOTG	-38.608088472	145.590859500	51.779	TRM57971.00	Trim. netR5
YALL	-38.182095389	146.349026167	64.740	TRM55971.00	Trim. netR9
YANK	-38.812266167	146.206895528	29.787	LEIAX1202GG	Leic. GRX1200GG
YRRM	-38.565158306	146.675193889	35.661	TRM57971.00	Trim. netR5

Table 2. Location, receiver type and antenna type of the GPSnet CORS stations used in this research. EBNK, LCLA, MAFF, WORI and YALL were also used to evaluate the PPP and PPP+Ion solutions.

The histogram of differences between the ionospheric delay measured at monitoring stations and ionospheric delays interpolated from nearby stations is shown in Figure 2.

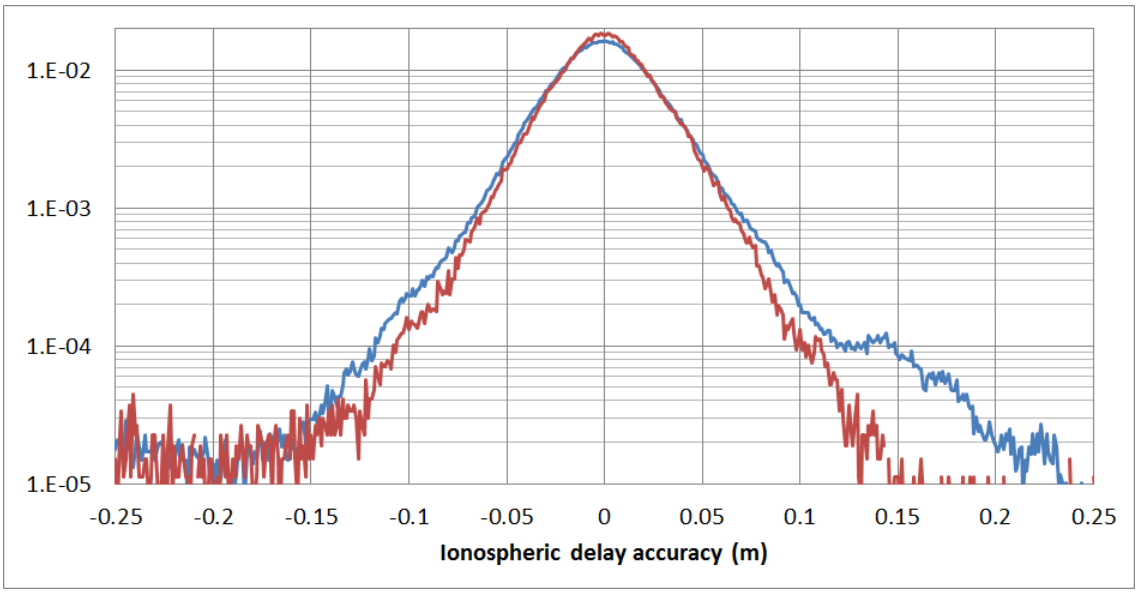

Figure 2. Differences between measured and interpolated ionospheric delay estimates. The ionospheric delay estimates were computed based on CLK91(red) and MADOCA (blue) products.

The red line corresponds to the ionospheric delays computed based on CLK91 products, while the blue line corresponds to the MADOCA products. More than 85% of the interpolated ionospheric corrections lie within ±5 cm or the measured values.

3.2 Ionospheric delay interpolation and Outlier rejection

For small the network used in this research, transmitting a base grid, station position and ionospheric delay calculated at each station, is a practical strategy. For networks covering large areas, it will be more efficient to map the ionospheric delays onto regular grid maps grid maps (a 1°× 1° square grid for example) for transmission.

In this study the measured ionospheric delays were grouped into satellite ionospheric delays and broadcasted using an NTRIP caster. The ionospheric message corresponding to one satellite included the ionospheric delays measured at all stations for which the satellite was visible. The station positions were provided in advance to the receiver software.

The receiver software estimated the ionospheric delay by performing a bilinear regression through a least squares method,

$$I_{sta} = I_0 + dI_{lat}(lat_{sta} - lat_0) + dI_{lon}(lon_{sta} - lon_0) \quad (7)$$

where, I_{sta} stands for the slant ionospheric delays measured at each station. I_0, d_{lat} and d_{lon} are the coefficients of the bilinear fit to the station ionospheric delays. The receiver's approximate position will be used as the origin (lat_0, lon_0) for the linear regression.

Although not evident in Figure 2, there were outliers in the ionospheric delays measured at some of these stations. Since most of these outliers appeared in stations other than the monitoring stations their effect is not visible in figure 2.

In order to detect and remove these outliers, an integrity monitoring algorithm was included in the Ionosphere interpolation algorithm:

1) Stations within 150km of the origin (monitoring station position) were selected.
2) Satellite single differencing was applied to the ionospheric corrections.
3) Bilinear regression and its corresponding mean square error was calculated for each satellite pair.
4) If the mean square error was below a threshold (10 cm), then I_0 was used as ionospheric delay estimate.
5) If not, bilinear regression was calculated using N_{sta} sets of N_{sta}-1 measurements, each missing one station. Here N_{sat} is the number of stations for which the ionospheric delay measurement exists.
6) The set with minimum mean square errors was selected.
7) If the new mean square error was below threshold, I_0 was used as ionospheric delay estimate.
8) If not, steps 5) to 7) were repeated.
9) If the minimum square error was above the threshold after two stations were discarded, the ionospheric delay estimation will be abandoned.

Tables 3 and 4 show the results of the interpolation and outlier rejection results.

	0 disc	1 disc	2 disc	no-output	resid (cm)
EBNK	74%	24%	0.5%	2%	2.57
LCLA	75%	23%	0.4%	2%	2.54
MAFF	76%	22%	0.4%	2%	2.59
WORI	75%	22%	0.4%	2%	2.60
YALL	75%	23%	0.4%	2%	2.56

Table 3. Outlier rejection results. Ionospheric delay based on CLK91

	0 disc	1 disc	2 disc	no-output	resid (cm)
EBNK	48%	38%	5%	8%	3.15
LCLA	54%	36%	4%	6%	3.31
MAFF	53%	37%	4%	6%	3.25
WORI	51%	39%	5%	5%	3.25
YALL	54%	36%	4%	6%	3.29

Table 4. Outlier rejection results. Ionospheric delay based on MADOCA

The first column of Tables 3 and 4 list the monitoring stations; the second column shows the percentage of cases without outliers; the third and fourth column show the percentage of cases with one and two outlier stations, respectively; the fifth column presents the percentage of cases were the ionosphere interpolation was abandoned. The mean square of residuals for when the interpolation was successful is presented in the last column, and plotted in Figure 3.

An average of 6.68 and 6.59 satellite pairs had ionospheric delay estimates for CLK91 and MADOCA, respectively. For 75% (CLK91) and 51% (MADOCA) of the cases, the mean square errors were below 10 cm without discarding any station measurements. For 98% (CLK91) and 93% (MADOCA) of the cases, the ionospheric delay measurements were successfully fitted into a bilinear function with less than 10 cm of means residuals after discarding one or two outliers. If using the mean square residuals of a bilinear regression as indicators, the expected accuracy of the single differenced ionospheric delay would be 2.57 cm when using CLK91, 3.24 cm when using MADOCA.

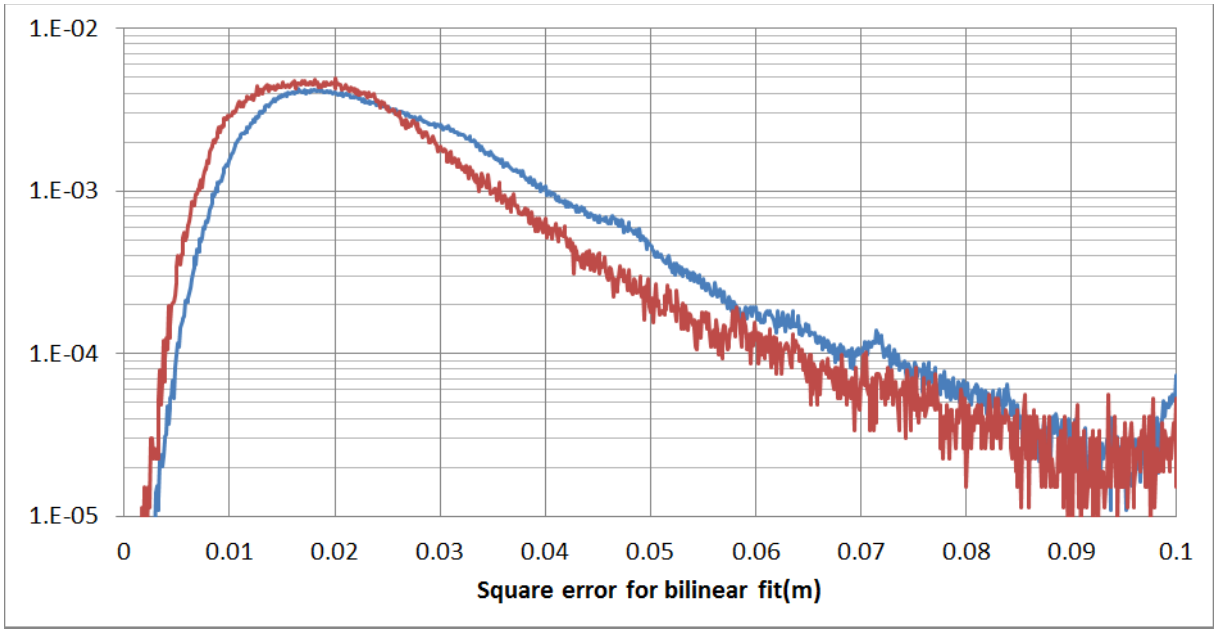

Figure 3. Mean Square errors of bilinear fit for ionospheric delays. Ionospheric delays were calculated based in CLK91 (blue) and MADOCA (red) products.

3.3 PPP and PPP+Ion positioning

Real-time kinematic PPP and PPP+Ion positions were calculated for the five monitoring stations mentioned in previous sections. The PPP solutions were set to restart every 3 hours, in order to evaluate the convergence time. The result presented here are statistics calculated from a total of 230 CLK91 and MADOCA based solutions from 31st August to 04th September 2016.

Figure 4 and Figure 5 show one of the solutions computed between 12:00 and 15:00 UTC on 1st September 2016. At YALL station. The PPP solutions are shown in red, PPP+Ion solutions are shown in blue.

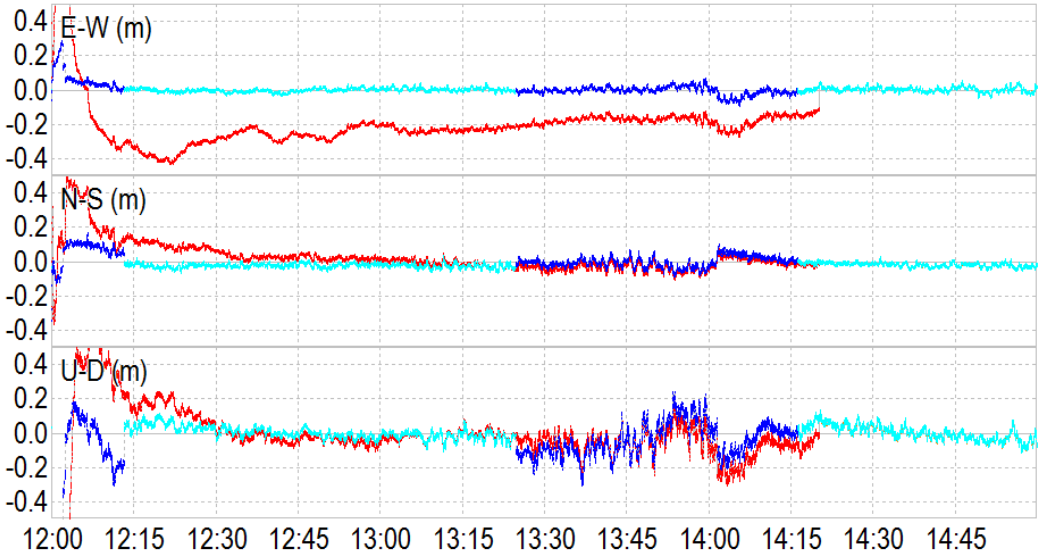

Figure 4. Example of PPP (red) and PPP+Ion (blue) positioning solutions using CLK91 products. Dark line corresponds to unfixed solutions, light line corresponds to ambiguity fixed solutions.

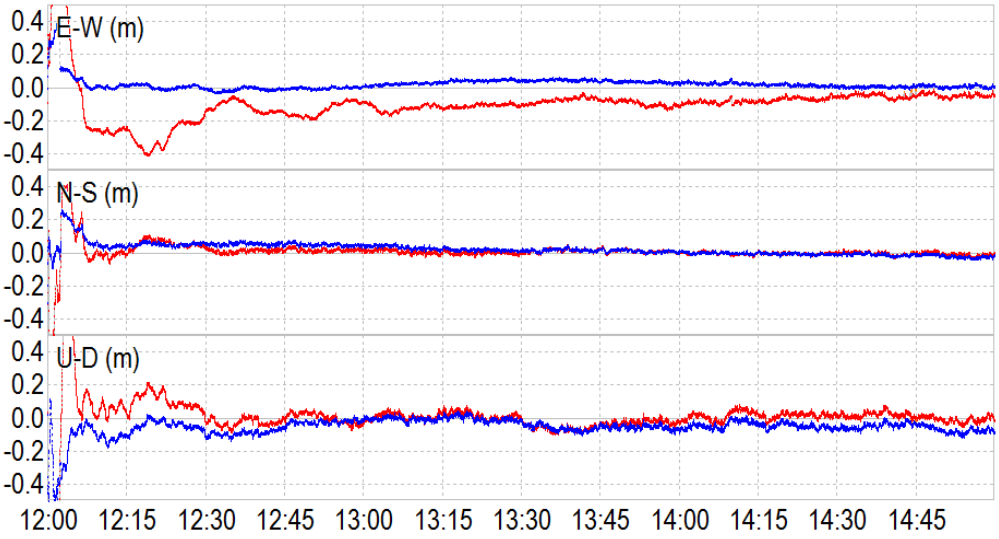

Figure 5. Example of PPP (red) and PPP+Ion (blue) positioning solutions using MADOCA products.

Both the CLK91 and MADOCA based solutions show an improved accuracy for the PPP solution on the first 15 minutes of convergence due to the use of ionospheric corrections. For the MADOCA PPP+Ion solution, both horizontal and vertical components converge to about 23 cm after the first 2.5 minutes when the first N_{WL} ambiguities were fixed. By comparison, MADOCA based PPP the RMS errors for the horizontal and vertical positions are above 65 cm at 2.5 minutes of convergence.

In the case of the CLK91 based solution, PPP+Ion solutions converge within 12.5cm of the vertical and horizontal accuracy, which allows the solution to fix more than 5 ambiguities at 14 minutes and reducing horizontal accuracy to better than 5 cm. By comparison CLK91 based PPP solutions had horizontal errors in excess of 20 cm for the first 30 minutes of convergence. The quality of PPP and PPP+Ion solutions based on CLK91 products is illustrated in Figure 6 and Table 5. They present the percentage of solutions that have position accuracy better than 10 cm at any given time of convergence.

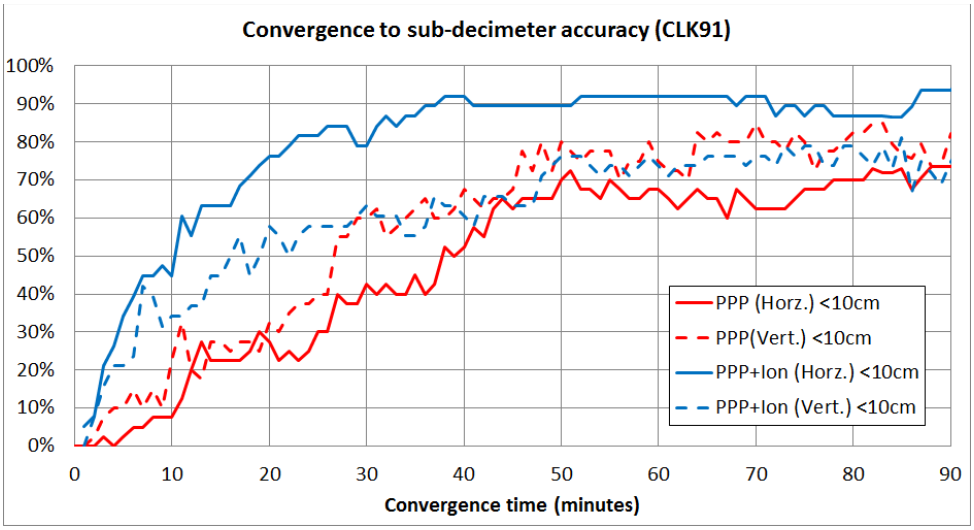

Figure 6. Percentage of solutions with Vertical (dashed) and Horizontal (solid) RMS errors below 10 cm for different times of convergence. Red lines represent CLK91 based PPP solutions; blue lines represent CLK91 based PPP+Ion solutions.

	2 min	5 min	10 min	15 min	30 min
Horizontal <10cm (PPP)	0%	3%	8%	30%	43%
Horizontal <10cm (PPP+Ion)	21%	39%	61%	63%	84%
Vertical <10cm (PPP)	8%	15%	32%	33%	63%
Vertical <10cm (PPP+Ion)	16%	23%	34%	50%	61%

Table 5. Convergence to 10 cm accuracy for PPP and PPP+Ion solutions based on CLK91 corrections

A significant improvement can be seen in the convergence time of horizontal positions especially during the first 30 minutes. Most solutions have sub-decimetre horizontal accuracy after 10 minutes of convergence. Convergence improvements are not as clear for the vertical component, with an average gain of 10% to 20% over the first 20 minutes but diminishing returns after that. It is known that the main reason that vertical accuracies are worse than horizontal accuracy is the high correlation between the clock errors and the vertical component. This situation can only be rectified when the satellite geometry changes. For cases were the high correlation between receiver clocks and vertical position are the main source for position errors, the inclusion of ionospheric corrections will have limited effect. A stronger modelling of clocks and position may be needed instead.

The performance of MADOCA based PPP and PPP+Ion solutions is illustrated in Figure 8 and Table 6. They present the percentage of MADOCA based solutions that have position accuracy better than 10 cm at any given time of convergence.

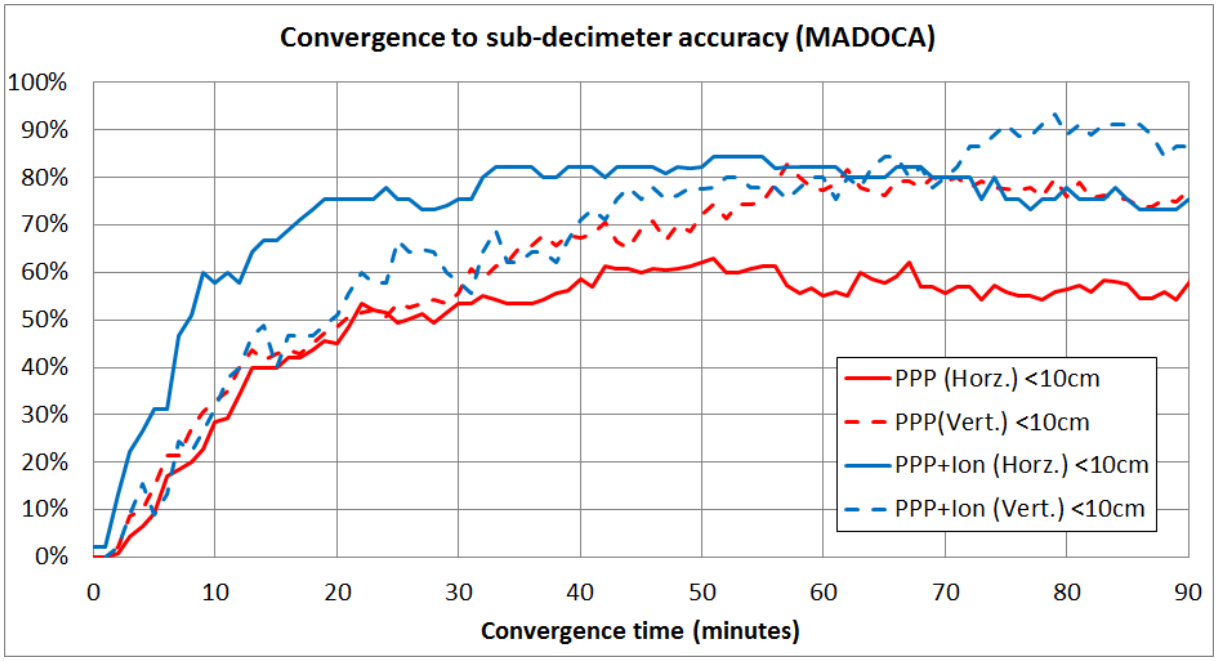

Figure 8. Percentage of solutions with Vertical (dashed) and Horizontal (solid) RMS errors below 10cm for different times of convergence. Red lines represent MADOCA based PPP solutions, blue lines represent PPP+Ion solutions.

	2 min	5 min	10 min	15 min	30 min
Horizontal <10cm (PPP)	0.7%	9%	28%	40%	53%
Horizontal <10cm (PPP+Ion)	13%	31%	58%	67%	76%
Vertical <10cm (PPP)	2%	15%	32%	43%	55%
Vertical <10cm (PPP+Ion)	9%	13%	38%	47%	56%

Table 6. Convergence 10 cm accuracy for PPP and PPP+Ion solutions based on MADOCA corrections

As in the case of CLK91 based solutions, significant gains can be seen in the horizontal accuracy with most of the solutions converging to sub-decimetre level before 10 minutes. In the MADOCA case however, there is no appreciable gain on the vertical component. Also, the percentage of decimetre level solutions is capped at about 80%. Because MADOCA has only recently included the real-time phase biases for ambiguity resolution for PPP, the accuracy of these products gave rise to low ambiguity resolution rates. This in turn limits the steady state accuracy of positioning solution to the decimetre level.

5. SUMMARY AND DISCUSSION

When considering CORS infrastructure for high precision positioning, two positioning techniques with different advantages are available. The differential technique, represented by RTK has fast convergence to centimetre level position. However RTK has high dependency on local ground infrastructure. The PPP technique, which can cover wide area with sparse CORS network. An ideal approach to build a positioning infrastructure to cover wide areas is to have RTK like systems for regions where CORS infrastructure is available, and a PPP system as backdrop. This paper present a case study for developing such system using existing global PPP correction products, e.g., CLK91 from CNES and MADOCA from JAXA, and local ionospheric corrections generated from a CORS network in Victoria, Australia.

A local CORS network presented in this research that has an average inter station spacing of 60 km could generate ionospheric delays with estimated accuracies of 3.3 cm or better. The global PPP solutions, augmented by these local ionospheric corrections show significant improvement in the convergence time for the horizontal component. Most solutions converge to sub-decimetre level in 10 minutes.

By using existing global PPP corrections, countries or regions without access to the CORS networks could utilise the corrections for high accuracy positioning. In particular, JAXA's MADOCA system has been tested for transmission over the QZSS LEX signal (JAXA, 2014) and is currently being considered for transmission once the system is operational. If this is the case, East-Asia and Oceania countries within the footprint of QZSS satellites will have access to this system.

ACKNOWLEDGEMENTS

This research is funded through the Australian Cooperative Research Centre for Spatial

Information (CRCSI Project 1.22) and is a collaborative project between the CRCSI and the Japan Aerospace Exploration Agency (JAXA). The CRCSI research consortium consists of Geoscience Australia, Land Information New Zealand, RMIT University, Victoria Department of Environment, Land, Water & Planning, Position Partners Pty. Ltd. and Fugro Satellite Positioning Pty. Ltd. The authors would also like to thank JAXA for maintaining the MADOCA real-time streams and the CNES for maintaining the CLK91 real-time. Finally the authors would like to thank GPSnet for providing data from reference and monitoring stations used in this study.

REFERENCES

Boehm J., Niell A., Tregoning P., Schuh H., "Global Mapping Function (GMF): A new empirical mapping function based on numerical weather model data", Geophysical research Letters, Volume 33, Issue 7 April 2006.

Chang, X. W., Yang X., Zhou T. (2009), "MLAMBDA: a modified LAMBDA method for integer least-squares estimation", Journal of Geodesy, Vol. 79, No 9, 2005, p 552-565

Ge M., Gendt G., Rothacher M., Shi C., Lui J., (2007), "Resolution of GPS carrier-phase ambiguities in Precise Point Positioning (PPP) with daily observations," Journal of Geodesy, vol. 82, pp. 389–399, 2007.

IGS, (2015). "Real-time Service", http://rts.igs.org/, Accessed September 2015.

JAXA, (2014), "Interface Specification for QZSS (version 1.6)". http://qz-vision.jaxa.jp/USE/is-qzss/DOCS/IS-QZSS_15D_E.pdf, November 2014

Kouba, J., (2009), "A Guide to using International GNSS Service (IGS) Products", http://igscb.jpl.nasa.gov/components/usage.html, Accessed October 2009.

Laurichesse D., Mercier F., Berthias J., Broca P., Cerri L., (2009), "Integer Ambiguity Resolution on Undifferenced GPS Phase Measurements and Its Application to PPP and Satellite Precise Orbit Determination," NAVIGATION: Journal of The Institute of Navigation, vol. 56, pp. 135 - 149, 2009.

Li, X., Ge, M., Dousa, J., Wickert, J. (2014): Real-time precise point positioning regional augmentation for large GPS reference networks. - *GPS Solutions,* vol. 18, 1, p. 61-71.

Zhang, H., Gao Z. Ge M., et. al. (2013), "On the Convergence of Ionospheric Constrained Precise Point Positioning (IC-PPP) Based on Undifferential Uncombined Raw GNSS Observations". *Sensors 2013, vol. 13, pp:15708-15725*

Zumberge, J. F., Heflin M. B., Jefferson D.C., Watkins M. M. Webb F. H., (1997). "Precise Point Positioning for The Efficient and Robust Analysis of GPS Data from Large Networks", Journal of Geophysical Research, 102, B3, 5005-17.